Chemical Engineering Science 161 (2017) 187–197

Contents lists available at ScienceDirect

Chemical Engineering Science

journal homepage: www.elsevier.com/locate/ces

DEM-CFD investigation of particle residence time distribution in top-spray fluidised bed granulation

Matthias Börner [b,*], Andreas Bück [a], Evangelos Tsotsas [a]

[a] NaWiTec, Thermal Process Engineering, Otto-von-Guericke University Magdeburg, Universitätsplatz 2, 39106 Magdeburg, Germany
[b] Hüttlin GmbH, A Bosch Packaging Technology Company, Hohe-Flum-Str. 42, 79650 Schopfheim, Germany

HIGHLIGHTS

- DEM-CFD simulation of a three phase fluidised bed based on similarity models.
- Particle residence time distributions are obtained for a top-spray fluidised bed.
- Deriving overspray ratios from the droplet existing time.
- Three types of particle wetting mechanisms are identified in the spray zone.

GRAPHICAL ABSTRACT

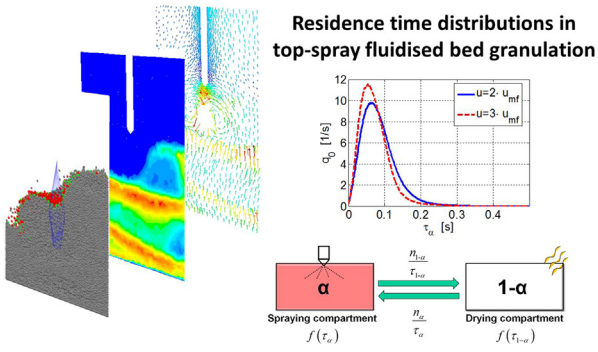

ARTICLE INFO

Article history:
Received 11 February 2016
Received in revised form 21 September 2016
Accepted 8 December 2016
Available online 19 December 2016

Keywords:
Fluidised bed
Top-spray
Wet granulation
Overspray
DEM-CFD
Similarity models

ABSTRACT

Numerical simulations in process engineering become more and more to a powerful tool in process optimisation and for improvement of process understanding. For multiphase flows, like fluidised bed granulation as a three phase system, the dynamics can be described by the coupled approach between the Discrete Element Method (DEM) for the solid and liquid phase with Computation Fluid Dynamics (CFD) for the gas phase. A key challenge in this simulation approach is given by the huge number of single particles in the original system. In order to run a three-phase top-spray fluidised bed by the coupled DEM-CFD in reasonable time scales, a scaling approach based on similarity models has been applied. Within the top-spray fluidised bed particle and droplet motions are investigated in a two-compartment approach, considering a spray and a drying zone. It can be shown that different particle crossing lengths and particle velocities through the spray zone lead to a particle residence time distribution with crucial impact on particle wetting and thus growth behaviour. In addition top-sprayed droplets are respected to obtain droplet existing time distributions and therefrom overspray ratios. Concluding from the results different particle wetting procedures in the spray zone are identified and discussed.

1. Introduction

Fluidised beds are a common technology in food, chemical and pharmaceutical manufacturing to produce granules from powder raw materials to improve powder properties for e.g. dosing, transportation and compressibility. In industrial applications different fluidised bed technologies can be differentiated according to the location of spray nozzle (top-spray, bottom-spray, Wurster, etc.) with each single technology having its advantages in certain granulation processes. Top-spray is commonly applied for agglomeration and layering of fine powders, Wurster for particle

* Corresponding author.
E-mail address: Matthias.Boerner3@Bosch.com (M. Börner).

http://dx.doi.org/10.1016/j.ces.2016.12.020
0009-2509/

Nomenclature

F_{pp}	inter-particle force [N]	u	particle velocity [m s^{-1}]
F_c	contact force [N]	T	torque [N m]
F_d	drag force [N]	v	gas velocity [m s^{-1}]
D	distribution function [–]	t	time [s]
g	gravitational constant [m s^{-2}]	V	volume [m^3]
i,j	indices [–]	V_{cell}	cell volume [m^3]
J	moment of inertia [kg m^2]	β_m	inter-phase momentum transfer coeff. [kg m^{-3} s]
m	mass [kg]	ϵ	bed porosity [–]
N_p	particle number [–]	ϵ_p	particle volume fraction [–]
N_s	number sample points [–]	ρ_g	gas density [kg m^{-3}]
p	pressure [Pa]	τ_g	stress tensor of the gas phase [Pa]
r	radius [m]	ω	angular velocity [rad s^{-1}]
S_p	sink term [N m^{-3}]		

coating or layering and bottom-spray can be used for both types of granulation.

In the top-spray configuration the spray nozzle is positioned in the upper part of the fluidised bed spraying liquid counter-currently to the fluidisation gas flow. Wetting of the fluidised powder occurs close to the spray nozzle. In all other areas of the fluidised bed drying takes place. The characteristic sub-processes of wetting and drying led to a process separation into two compartments, a spray zone and a drying zone. This process separation was first introduced by Sherony (1981) and Wnukowski (1989), and has been further investigated and applied in recent years, especially in the description of granulation processes by population balance models (Hoffmann et al., 2011; Li et al., 2012; Hussain et al., 2014; Chaudhury et al., 2015).

Due to the counter-current and turbulent flow condition around the spray nozzle in the top-spray fluidised bed, the description of wetting and particle growth mechanisms is relatively complex. Particle wetting mainly depends on the fluidisation conditions and, thus, on the particle motion through the spray zone, on the relative velocity between droplets and particles as well as on the spatial distribution of particles in the freeboard domain. In order to define compartments, an earlier work has already described (Börner et al., 2011) the demarcation of a spray zone for different fluidised bed technologies. The spray zone demarcation describes the spatial domain in which active droplets occur, that can collide with fluidised particles, finally leading to a successful wetting event.

Spray zone dimensions in the top-spray fluidised bed were derived from high granular temperatures close to the tip of the spray nozzle, measured by Particle Image Velocimetry (PIV) in a pseudo 2-D fluidised bed. Turchiuli et al. (2011) obtained spray zone dimensions by temperature and humidity profiles in a top-spray fluidised bed. Later, spray zone dimensions have also been determined by measurements of the spatial existence of droplets in a cylindrical top-spray fluidised bed, utilising a conductivity probe (Börner et al., 2014).

The particle residence time distribution in the spray zone, which is the interaction time of particles with active droplets, is a key influence on the wetting distribution and consequently for particle growth in granulation. Since those process variables are difficult to measure, an alternative can be a multiphase process simulation by a coupled DEM-CFD approach.

Computational investigations for laboratory-scale fluidised bed granulators have already been presented by different authors (Fries et al., 2011, 2013; Li et al., 2015). The solids are considered by the Discrete Element Method (DEM) and the fluid by Computation Fluid Dynamics (CFD). However, solid materials in production-scale fluidised beds usually consist of billions of single particles. These extreme particle numbers require huge computational work in the DEM to resolve the interactions between the solid particles, usually at time steps of ca. 10^{-6} s.

Such large particle numbers therefore still present a challenge in simulation of process behaviour on reasonable time scales, as required for instance, for design and troubleshooting of processes. A reduction of simulation times can either be achieved by a reduction of computed particle interactions (Mio et al., 2009) or by computer hardware improvements (Radeke et al., 2010). These techniques show great promise, but are still not sufficient to simulate extreme particle numbers in production-scale systems.

Alternatively, the number of particles can be reduced, for instance by increasing the particle size. In the consequence this also changes the process dynamics. In gas-solid systems, the increase of particle size tremendously affects the drag force on the particles in the fluid flow. That makes linear scaling not applicable. A possible scaling method has been proposed by coarse grain models (Sakai and Koshizuka, 2009; Sakai et al., 2014). In these models a group of fine particles is considered as a single particle. The drag model and the contact forces are adapted according to the scaled particle size. Washino et al. (2007) have presented a particle scaling based on similarity models. In their approach they selected dimensionless parameters derived from governing equations of the fluid and particles are kept constant. Those models account for different hydrodynamic behaviour of scaled particles in a fluid flow, however, they can only be applied to gas-solid systems, where the fluid force is dominant compared to energy dissipation during inter-particle collisions, an appropriate assumption in fluidised beds. The contact model, in which the contact stiffness is dependent on the particle size (Thakur et al., 2016) is not considered in this scaling approach. A disadvantage of particle scaling is that increased particle sizes always come along with reduced spatial resolution of particle distributions and dynamics.

Within the frame of performed simulations of fluidised bed granulation the spray of liquid has been considered. Such considerations in DEM simulations have been previously shown by Suzzi et al. (2012) for tablet coating and in DEM-CFD simulations by Fries et al. (2011). Both introduced a liquid containing spray domain. Particles or tablets passing this domain gain a certain amount of liquid. Single droplets have not been accounted for. A consideration of sprayed droplet elements will add a second discrete phase to the simulation approach. Droplets are in a lower scale to the discrete particle elements. Since huge numbers of sprayed droplets are presented in a conventional spray process, such simulation approach become computationally very expensive. Sutkar et al. (2016) have presented this three-phase approach of

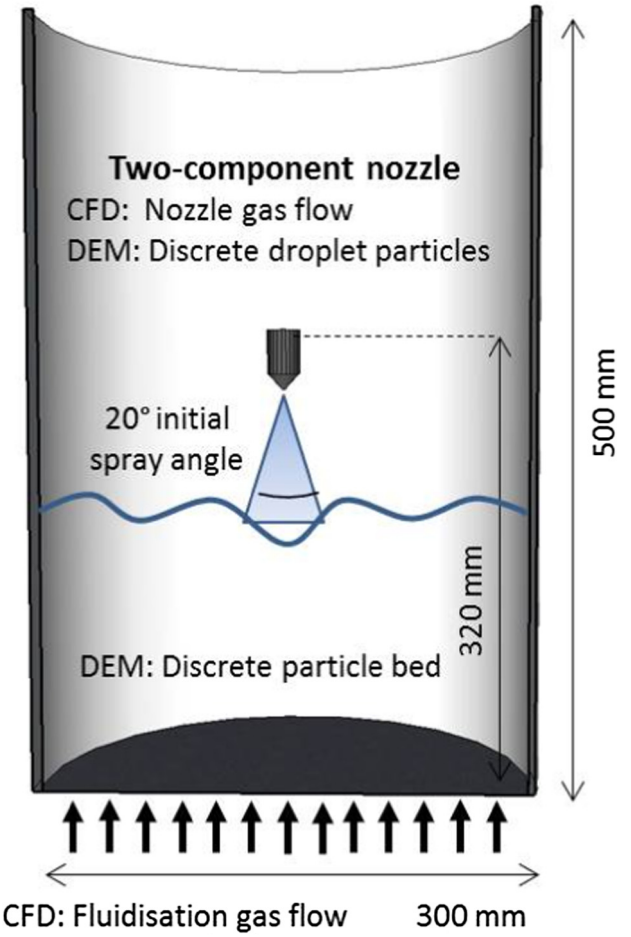

Fig. 1. DEM-CFD simulation domain of the top-spray fluidised bed.

gas, droplet and particle flow for a 2-D sprout fluidised bed with draft plates. By applying the scaling approach to the discrete elements in the presented work a cylindrical laboratory-scale fluidised bed has been simulated applying typical granulation conditions.

Based on a previous experimental work (Börner et al., 2014), the scope of this study was to extend the findings of mean particle residence times within a two-compartment approach to obtain residence time distributions of particles and existing time distributions of droplets in a three-phase top-spray fluidised bed. The focus is particularly on the spray zone to improve the understanding of particle wetting and growth mechanism within the top-spray configuration. A simple collision model for droplet has been introduced to study droplet-particle wetting events and distribution of wet particles in the bed.

2. Material and methods

2.1. Top-spray fluidised bed

The geometry of an experimentally investigated top-spray fluidised bed in a previous work (Börner et al., 2014) has been used within the frame of this simulation study. The fluidised bed is of cylindrical shape having an inner diameter of 300 mm and a height of 500 mm. The top-spray nozzle has been adjusted in a height of 320 mm above the gas distributor. The two-component nozzle (Schlick 970-S8) has been simplified in the simulations by a circular gas outlet of 2 mm and a cylindrical nozzle body. Fig. 1 shows the different process domains in the fluidised bed. The simulated particle material are γ-Al_2O_3 spheres of Geldart class D. The spheres have a mean particle size of $d_p = 1.8$ mm and a density of $\rho_p = 1040\ \mathrm{kg/m^3}$. The minimum fluidisation velocity has been determined at $u_{umf} = 0.56$ m/s according to the equation of Kunii and Levenspiel (1991).

2.2. DEM-CFD simulation

2.2.1. Models

The fluidised bed has been simulated in an Eulerian coupling between the DEM and the CFD. The DEM follows the Lagrangian approach of discrete elements moving within a certain domain; its theory goes back to Cundall and Strack (1979). The motion of each particle i in the process chamber is described by Newton's second law of motion:

$$m_i \frac{\mathrm{d}\mathbf{v_i}}{\mathrm{d}t} = V_i \nabla p + \frac{V_i \beta_m}{\epsilon_p}(\mathbf{u} - \mathbf{v}) + m_i \mathbf{g} + \mathbf{F_{c,i}}. \quad (1)$$

The forces acting on each particle have been modelled according to Deen et al. (2007), including all fluid forces. The forces are the pressure gradient of the fluid, the drag force, the gravitational force, the contact forces between all contact partners. Contact-less interparticle forces like electrostatic forces have been neglected. The drag force has been determined according to Di Felice (1994). Besides translational motion, the angular momentum needs to be considered:

$$J_i \frac{d\boldsymbol{\omega_i}}{dt} = \mathbf{T_i} \quad (2)$$

with $J_i = \frac{5}{2} m_i r_i^2$ for spherical particles. In order to consider the interparticle interaction and between particles and apparatus walls, the Hertz-Mindlin contact model (Mindlin and Deresiewicz, 1953) has been used. To consider the droplets, modelled as discrete particles in the DEM, the contact model has been extended: In the droplet contact model it is assumed that every droplet particle that collides with the wall or with another particle will be deposited on the surface or wall. After the collision event the droplet particle is deleted. Droplet particles leaving the simulation domain, e.g. by elutriation, are deleted as well. All collision events of each particle are stored in a counter variable, to distinguish between particle-particle, particle-wall and particle-droplet collisions. From the counter variables, the number of all collided or deposited droplets can be determined then.

For the gas phase the discretized, volume-averaged Navier-Stokes equation

$$\frac{\partial}{\partial t}\left(\epsilon \rho_g \mathbf{v}\right) + \nabla\left(\epsilon \rho_g \mathbf{v}\mathbf{v}\right) = -\epsilon \nabla p + \nabla(\epsilon \boldsymbol{\tau_g}) + \epsilon \rho_g \mathbf{g} - \mathbf{S_p}. \quad (3)$$

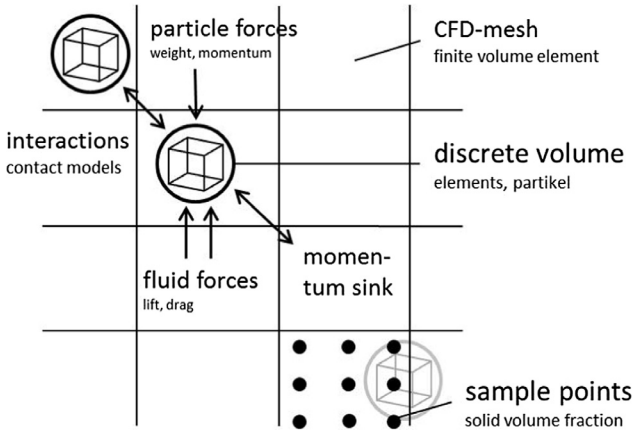

Fig. 2. Simplified principle of DEM-CFD simulations.

Table 1
Settings in the DEM-CFD simulations. The particle properties are for the test material γ-Al_2O_3 as reported in Antonyuk et al. (2010).

Parameter	Setting	Unit
CFD time step t_{CFD}	$2 \cdot 10^{-4}$	[s]
DEM time step t_{DEM}	$1 \cdot 10^{-6}$	[s]
Shear modulus G	$5.8 \cdot 10^{8}$	[N m^{-2}]
Poisson's ratio ν	0.25	[–]
Coeff. of restitution part.-part. e_n	0.735	[–]
Coeff. of restitution part.-wall e_n^w	0.735	[–]
Friction coeff. part.-part. μ	0.3	[–]
Friction coeff. part.-wall μ^w	0.3	[–]
Rolling friction part.-part. μ_r	0.01	[–]
Rolling friction part.-wall μ_r^w	0.01	[–]

has been solved in each volume element of the CFD mesh by a finite volume method. Besides mass conservation, the conservation of momentum needs to be fulfilled:

$$\frac{\partial}{\partial t}\left(\epsilon\rho_g\right) + \nabla\left(\epsilon\rho_g\mathbf{v}\right) = 0 \tag{4}$$

The turbulence of the incompressible fluid flow has been accounted for by the k-ϵ−model.

Fig. 2 schematically shows the DEM-CFD coupling approach between the CFD and DEM. The rectangular grid illustrates the CFD mesh of the fluid domain. Discrete elements moving and interacting with each other in this fluid domain with permanent force and energy exchange between both considered phases. The discrete elements are treated as obstacles in the fluid domain. To obtain the occupation of discrete elements per CFD mesh cell, each mesh cell is scanned by sample points N_s to determine the according solid volume fraction:

$$\epsilon_p = \frac{\frac{N_s}{N_p}\sum_{i=1}^{N_p} V_i}{V_{cell}} \tag{5}$$

To realise the consideration of the discrete elements (particles, droplets) in the fluid flow, a sink term S_p has been introduced in each mesh cell in the CFD:

$$\mathbf{S_p} = \frac{1}{V_{cell}}\int_{V_{cell}}\sum_{i=0}^{N_p}\frac{V_i\beta_m}{\epsilon_p}(\mathbf{v}-\mathbf{u_i})D(\mathbf{r}-\mathbf{r_i})\mathrm{d}V. \tag{6}$$

The DEM-CFD simulations have been performed using the coupling module between the DEM software package EDEM 2.3.1 and the CFD software Ansys Fluent 12.1.16. Table 1 summarizes all relevant settings in the DEM and CFD.

2.2.2. Validation of DEM-CFD simulation

The DEM-CFD models, previously presented in Section 2.2.1, needs to be validated against an experimental setup. Since three-dimensional cylindrical fluidised beds are very hard to analyse by measurements due to opacity of the multiphase flow, the flat pseudo-2D fluidised bed introduced in the previous work (Börner et al., 2014) has been used for validation here. The previous work further dealt with an experimental comparison between a flat and a cylindrical fluidised bed to confirm general applicability of such simplified geometry. It was shown that the flat fluidised bed can predict particle motions sufficiently. So, the considered flat fluidised bed can be seen as a centred cross section through the cylindrical fluidised bed. The flat fluidised bed has corresponding dimensions, having a width of 300 mm, a height of 500 mm and a bed depth of 20 mm. In the frame of validation, the spray nozzle is removed to concentrate on a bubbling fluidised bed filled with γ-Al_2O_3 particles. Digital Image Analysis (DIA) for the determination of the solid volume fraction ϵ_p and Particle Image Velocimetry (PIV) for the particle velocity v have been applied. The size of the flat fluidised bed allows direct DEM-CFD simulation with the real total particle number of approximately 165.000 alumina spheres, having a initial fixed bed height of 150 mm. For qualitative comparison of particle motion, Fig. 3 shows snapshots obtained from an experiment and a DEM-CFD simulation with identical particle size at a particle fluidisation velocity of $u = 2 \cdot u_{mf}$.

Fig. 4 shows the comparison of the time-averaged norm of the particle velocity and the solid volume fraction at bed heights of 100, 200 and 300 mm obtained in the experimental flat fluidised bed and in the corresponding DEM-CFD simulation. The profiles of the experiments with simulations show the same trend but possess a certain offset. The fluctuation in profiles from the simulations can be traced back to the simulation of only 5 s, being computationally expensive and time consuming. Other reasons are wall influence on particle motions in the measurements and non-modelled particle interactions, like electrostatic charging, adhesion or van der Waals forces in the contact model. However, dynamics and fluidisation behaviour of the particles can be sufficiently reproduced by the proposed DEM-CFD approach.

2.3. Similarity model

2.3.1. Scaling approach

As was mentioned earlier, the total numbers of particles and droplets have huge influence on the computational load, as for each particle or droplet the translational motion and rotation have to be calculated, and possible collision events need to be detected and resolved. The computational load of handling collisions scales roughly quadratically with the total number of particles and droplets. In order to decrease the computational load, total numbers need to be reduced while maintaining the process dynamics. One approach is scaling based on similarity models, where selected dimensionless numbers are kept constant across system scales according to the theory of similarity in fluid mechanics. This kind of similarity model has been applied by Link et al. (2009). They compared scale deviating experiments with results of DEM-CFD simulations. The idea of this approach has been followed within this work. This approach deviates from Wahino's similarity model. For scaling they used three dimensionless parameters (normalized acceleration of gravity, normalized particle density and Reynolds number) derived from the governing equations. Similarity conditions for particle diameter, superficial gas velocity, gas viscosity, gas density and particle density have been obtained. As a particularity the particle diameter scales linearly.

The target in applying similarity models is to significantly reduce computation time. However, in the scaling it is absolutely important not to change any flow behaviour. In the here proposed similarity model the conservation of mass as well as three dimensionless number has been applied. In order to consider the buoyancy of particles in the gas flow the Archimedes number Ar has been taken into account. The Ar number describes the ratio between the gravity and the friction force:

$$Ar = \frac{g d_p^3(\rho_p - \rho_g)}{\nu_g^2\rho_g}. \tag{7}$$

The Reynolds number Re respects the inertia force on the viscous force of the fluid:

$$Re = \frac{d_p u}{\nu_g}. \tag{8}$$

The drag force of particles referred on the friction force, described by the Stokes number St,

$$St = \frac{F_d}{\nu_g\rho_g d_p u}, \tag{9}$$

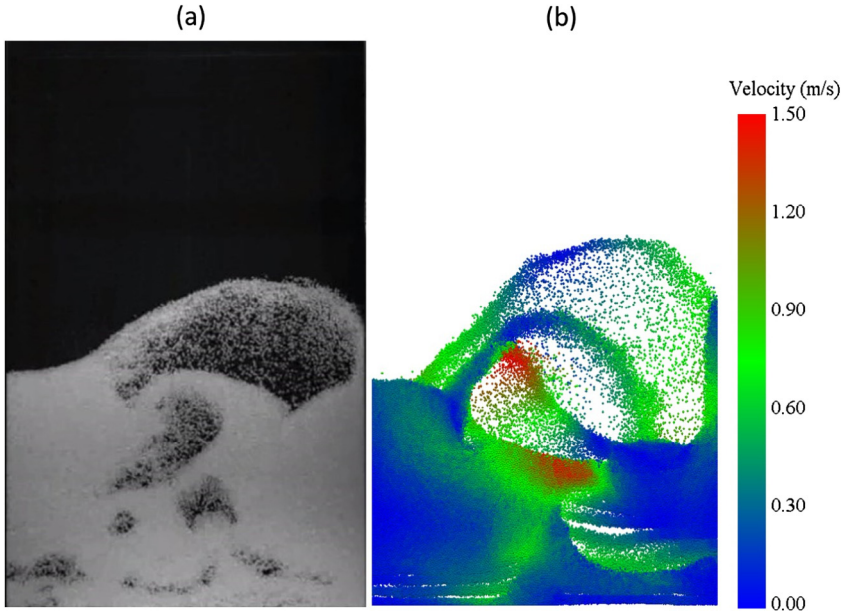

Fig. 3. Qualitative comparison of (a) an image of fluidised alumina spheres in the flat fluidised bed with (b) an image of the DEM-CFD simulation with identical particle number at $u = 2 \cdot u_{mf}$.

remains constant as well. F_d has been determined by the drag force correlation of Di Felice (1994), the same correlation as in the DEM-CFD coupling approach.

The scaling factor k_s describes the ratio of the reduced particle number $N_{p,2}$ in the simulation to the number of particles in the original system N_p by

$$k_s = \frac{N_{p,2}}{N_p}. \tag{10}$$

Applying mass, Ar and Re number conservation ($M_{bed,1} = M_{bed,2}, Ar_1 = Ar_2$ and $Re_1 = Re_2$) system properties need to be modified to fulfil the conditions. Since three equations are considered for scaling, three parameters for the fluid and the particles, all three contained in M_{bed}, Ar and Re number referred to as similarity conditions, have been selected and adapted. These parameters comprise the particle diameter d_p, the particle density ρ_p and the gas viscosity v_g. The conservation of St number has been used later to confirm equal flow conditions in the fluidised bed.

The scaled particle diameter $d_{p,2}$ for reduced particle numbers can be determined from the mass conservation:

$$d_{p,2} = \sqrt[3]{\frac{6m_{bed}}{\pi\rho_{p,2}N_{p,2}}}. \tag{11}$$

The bed mass m_{bed} is the sum of all single particle masses:

$$m_{bed} = N_p\rho_p\frac{\pi}{6}d_p^3. \tag{12}$$

The scaled particle density $\rho_{p,2}$ results from the conservation of Ar number:

$$\rho_{p,2} = \frac{d_p^3}{d_{p,2}^3}\frac{v_{g,2}^2}{v_g^2}(\rho_p - \rho_g) + \rho_g. \tag{13}$$

The scaled gas viscosity $v_{g,2}$ is determined from the conservation of Re number:

$$v_{g,2} = \frac{d_{p,2}}{d_p}v_g. \tag{14}$$

Inserting Eq. (14) in Eq. (13), Eq. (13) simplifies to:

$$\rho_{p,2} = \frac{d_p}{d_{p,2}}(\rho_p - \rho_g) + \rho_g. \tag{15}$$

Fig. 5 shows the scaled particle diameter and the particle density for reduced particle numbers. In Fig. 6 the gas viscosity for reduced particle numbers are presented.

In the cylindrical fluidised bed with an initial fixed bed height of 150 mm a total number of 2.084 million γ-Al_2O_3 particles are contained. To enable the simulation a scaling down by factor ≈21, i.e. $k_s \approx 1/21$, has been performed. Finally, 100,000 particles have been considered inside the fluidised bed. Besides the alumina spheres, liquid droplets in the spray have been assumed to be discrete particles as well considering a three-phase system consisting of a gas, liquid and solid phase. A liquid spray rate of 0.236 l/h is set in the simulation. Since the discrete particles are scaled in size, the droplets need to be scaled, too. The mean droplet size produced by the Schlick spray nozzle has been used as initial droplet size $d_{d,1}$. The scaling of the droplet size is dependent on the scaling of particles interlinked by the gas viscosity

$$d_{d,2} = d_{d,1}\frac{v_{g,2}}{v_{g,1}}. \tag{16}$$

The scaled droplet density results by the constant droplet Archimedes number Ar_d with

$$\rho_{d,2} = Ar_d\frac{v_{g,2}^2\rho_g}{d_{d,2}^3 g} + \rho_g. \tag{17}$$

Finally, a droplet creation rate of 1 million droplets per second have been considered in the simulation. All applied parameters in the simulation are shown in Table 2.

2.3.2. Validation of similarity model

As an extension to the validation of the DEM-CFD simulation approach, the validity of the similarity model has been proven by simulating two reduced particle numbers in the flat fluidised bed. All settings are the same as described in Section 2.2.2. The particle number has been scaled from originally 165,000 particles down to 100,000 and 40,000 particles. Fig. 7 shows the time-averaged solid volume fraction distribution after a total simulation

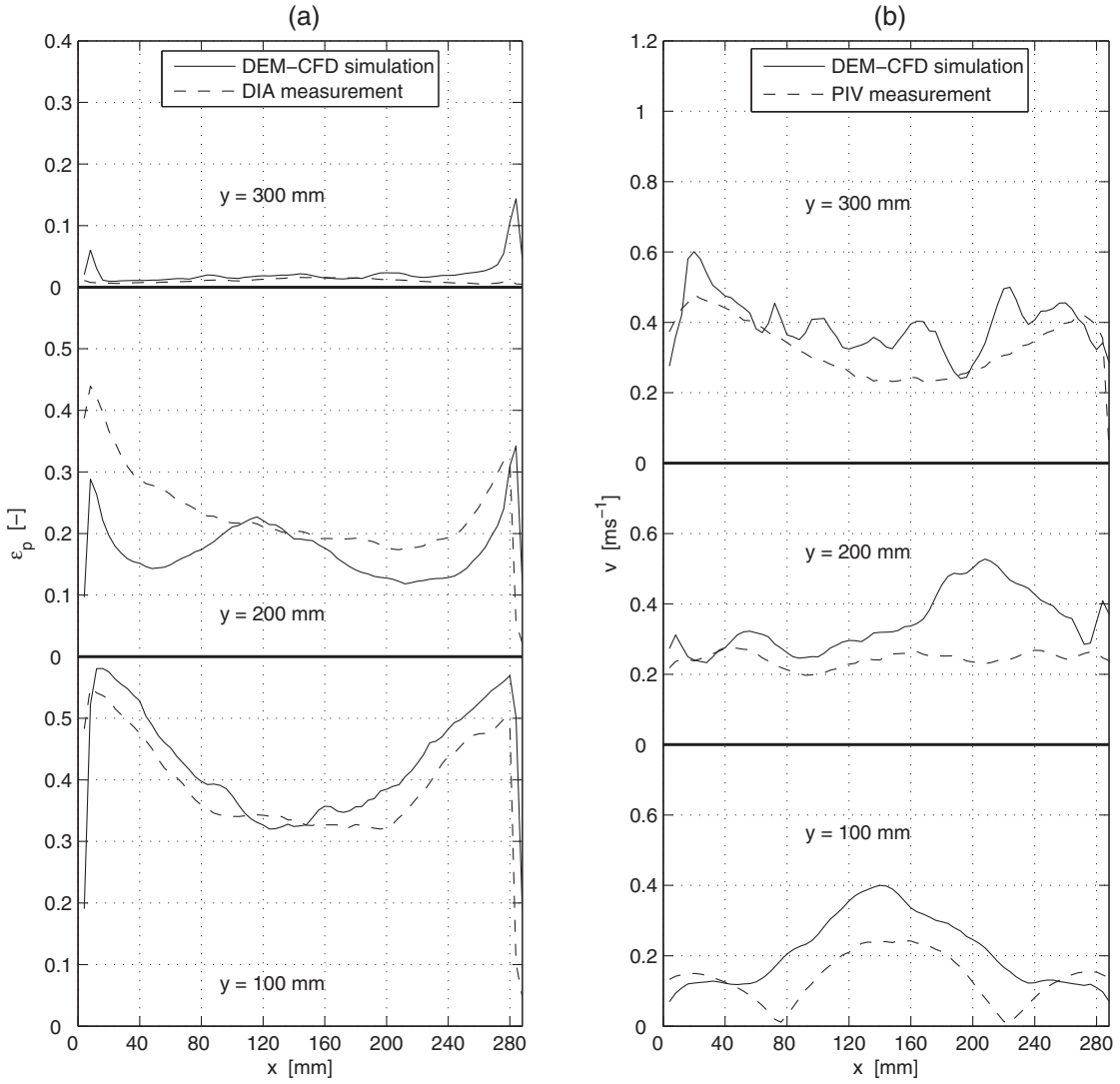

Fig. 4. Validation the DEM-CFD simulation in the flat fluidised bed proven with the (a) solid volume fraction experimentally obtained by DIA and (b) the norm of the particle velocity by PIV.

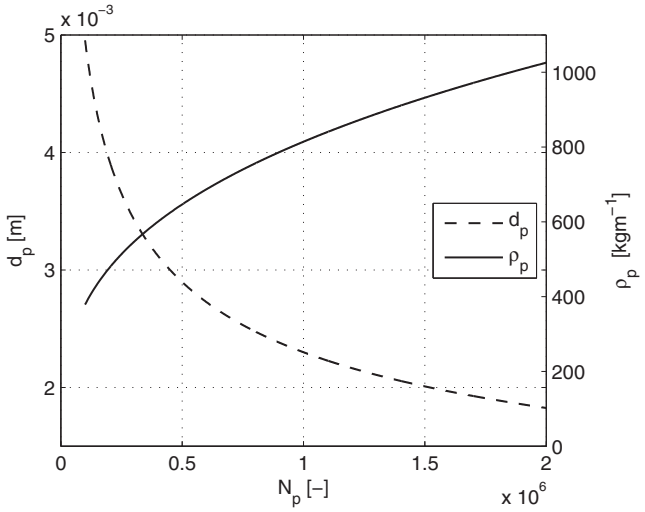

Fig. 5. Scaling dependence of particle diameter and particle density on the reduced particle number.

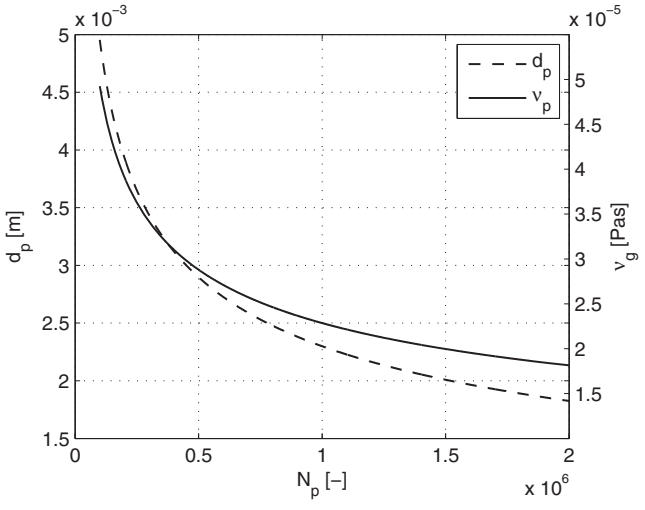

Fig. 6. Scaling dependence of particle diameter and gas viscosity on the reduced particle number.

Table 2
Particle and droplet parameter in the DEM-CFD simulations of the fluidised bed applying the scaling approach.

Parameter	Origin	Scaled	Unit
Particle number N_p	2,084,000	100,000	[–]
Scaling factor k_s	1	0.048	[–]
Particle diameter d_p	0.0018	0.00648	[m]
Particle density ρ_p	1040	289	[kg m^{-3}]
Gas viscosity v_g	$1.79 \cdot 10^{-5}$	$4.92 \cdot 10^{-5}$	[m^2 s^{-1}]
Droplet rate N_d	$2.37 \cdot 10^{6}$	$1 \cdot 10^{6}$	[s^{-1}]
Mean droplet size $d_{d,1}$	$3.75 \cdot 10^{-5}$	$10 \cdot 10^{-5}$	[m]
Water density ρ_l	1000	364	[kg m^{-3}]

time of 5 s. While scaling down particle number, the particle size increases and, thus, the local resolution of particle distribution decreases. However, the distribution pattern of solid volume fraction and the bed expansion remain the same. In Table 3 the mean solid volume fraction, the bed height and the mean particle velocity are listed to assess the similarity approach. The means solid volume fraction and the bed height almost stay constant. It becomes obvious that the mean particle velocity slightly drops at a lower particle number. With increasing particle size the particle contact area with the wall becomes larger. Wall friction becomes dominant being one of the critically discussed drawback of the flat fluidised bed which has now a negative impact on the particle dynamics. Despite of this effect, the proposed similarity model shows applicability to enable an effective reduction of particle number and thus a significant reduction of simulation time.

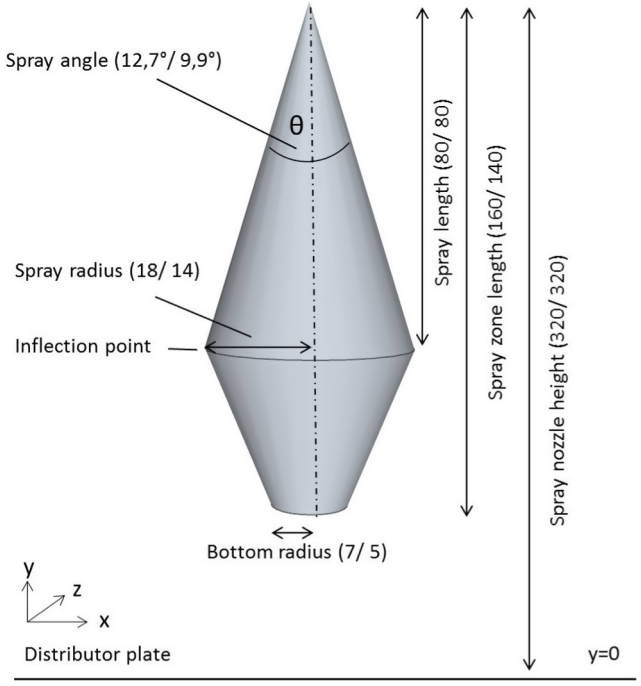

Fig. 8. Spray zone subgeometry in the top-spray fluidised bed for both fluidisation velocities. The numbers in brackets are the characteristic spray zone length in millimeter. The first number corresponds to $u = 2 \cdot u_{mf}$ and the second to $u = 3 \cdot u_{mf}$.

3. Results

Within the frame of the numerical simulation study two different superficial gas velocities at a constant nozzle liquid mass flow rate have been investigated for the top-spray fluidised bed. The superficial gas velocities of $2 \cdot u_{mf}$ and $3 \cdot u_{mf}$ have been chosen. In the context of granulation in the fluidised bed process a two compartment approach is applied dividing the system into a spray and a drying zone. The demarcation of the spray zone has been taken over from the experimental determinations of Börner et al. (2014) for the two equal fluidisation velocities as well as for the same nozzle gas flow rate of $\dot{M}_g = 3.6$ kg/h and the nozzle height of $h = 320$ mm above the gas distributor. The measured spray zone border lines have been simplified assuming to be a straight-line between the characteristic corner points. The corner points comprise the characteristic measures of the spray angle, the loca-

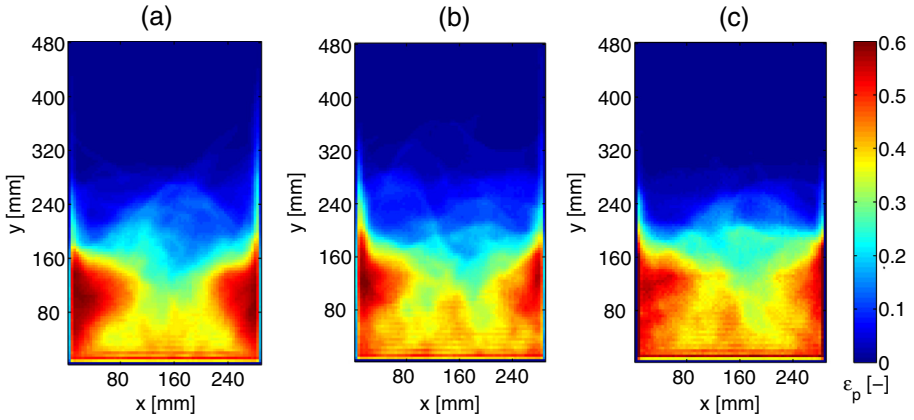

Fig. 7. Time-averaged solid volume fraction (a) 165,000 particles, (b) 100,000 particles and (c) 40,000 particles.

Table 3
Validation of the similarity model for three different particle numbers (165,000, 100,000 and 40,000).

Parameter	165,000	100,000	40,000	Unit
Scaling factor k_c	1	0.606	0.242	[–]
Mean solid volume fraction $\overline{\epsilon_p}$	0.168	0.1687	0.1684	[–]
Bed height $\overline{h}$	0.112	0.113	0.106	[m]
Mean particle velocity $\overline{v}$	0.37	0.36	0.32	[m s^{-1}]

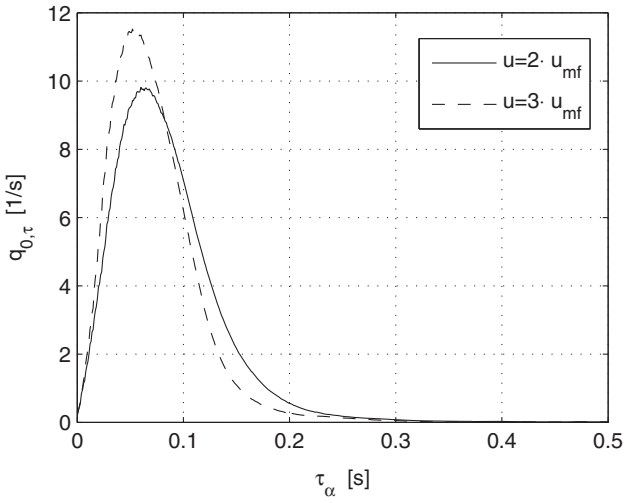

Fig. 9. Particle residence time distribution $q_{0,\tau}$ in the spray zone for superficial gas velocities $u = 2 \cdot u_{mf}$ and $u = 3 \cdot u_{mf}$.

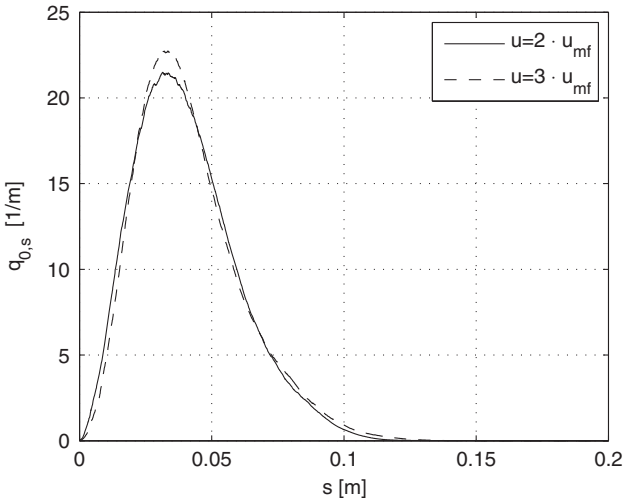

Fig. 10. Particle crossing length distribution $q_{0,s}$ through the spray zone for superficial gas velocities $u = 2 \cdot u_{mf}$ and $u = 3 \cdot u_{mf}$.

tion of the inflection point and the end of spray zone. The simplified spray zone, which is illustrated in Fig. 8, has been implemented as a sub-geometry into the DEM simulation framework.

In the DEM all temporal and spatial particle information can be accessed. Time and location of particles entering and leaving the spray zone sub-geometry have been recorded in the simulation. The time difference between entering and leaving describes the particle residence time τ_α in the spray zone. For all crossing particles in the total simulation time of 15 s, the particle residence time distribution has been obtained, presented as number density distribution in Fig. 9 for both investigated fluidisation velocities.

Particles stay in between 0 and 0.25 s in the spray zone, on average 0.052 s for $u = 2 \cdot u_{mf}$ and 0.04 s for $u = 3 \cdot u_{mf}$. Thus, the particle residence time depends on the fluidisation velocity. The fluidisation velocity determines the particle velocities and the spatial particle distribution in the entire zone. Basically, an increase of fluidisation velocity reduces the mean residence time in the spray zone. The obtained skewed distribution of particle residence time $q_{0,\alpha}$ can be well described by a Weibull distribution:

$$q_{0,\alpha}(\tau_\alpha) = ba^{-b}\tau_\alpha^{b-1} \cdot e^{(-\tau_\alpha/a)^b}. \tag{18}$$

The estimated Weibull parameters a and b are listed for both fluidisation velocities in Table 4.

Besides the particle residence time distribution, a particle crossing length distribution has been determined from the two particle locations of entering and leaving the spray zone. The crossing length as number density distribution is shown in Fig. 10. This distribution highlights that some particles cross the entire spray zone from the top to the bottom, some of them only cross from one side to the other one and some particles only touch the outer spray zone border. Contrary to the residence time, the crossing length is less affected by the fluidisation velocity. Most of all the fluidisation velocity determines the particle velocity and only to a lesser extent the particle flow pattern through the spray zone. Larger fluidisation velocity increases the bed porosity and thereby the bed height and the number of particles with longer crossing paths. The maximum particle crossing length increases from 75% of the spray zone length at $u = 2 \cdot u_{mf}$ to 87% at $u = 3 \cdot u_{mf}$. This basically corresponds to almost the entire spray zone length having larger exchange opportunities with sprayed droplets. Particles with very short crossing length have only few chances to come into contact with droplets.

From the DEM-CFD simulation further particle statistics are obtained, listed in Table 4, including the re-circulation times, which is the summation of the particle residence time in the spray zone τ_α and in the drying zone $\tau_{1-\alpha}$, the solid volume fractions ϵ_p, the mean particle velocities v and the mean crossing lengths l_α. These statistics confirm the findings that increased particle dynamics at larger gas velocities speed-up the re-circulation behaviour and shortens particle residence times and crossing lengths.

Besides the simulation of discrete particles at $u = 2 \cdot u_{mf}$ and $M = 3.6$ kg/h discrete droplets have been created in a small virtual volume below the gas outlet of the top-spray nozzle. After the droplet creation the droplets strictly follow the expanding nozzle gas

Table 4
Distributed particle dynamics in the spray zone obtained in the DEM-CFD simulations.

Parameter	$u = 2 \cdot u_{mf}$	$u = 3 \cdot u_{mf}$
Mean particle residence time in the spray zone τ_α	0.0524 s	0.0404 s
Max. particle residence time in the spray zone $\tau_{\alpha,max}$	0.227 s	0.208 s
Re-circulation time τ_{re}	58.5 s	51.1 s
Total particle passes N_α	1707 s^{-1}	1957 s^{-1}
Mean solid volume fraction in the spray zone α	$8.9 \cdot 10^{-4}$	$8 \cdot 10^{-4}$
Mean crossing length $\bar{l}_\alpha$	0.0307 m	0.0317 m
Max. crossing length $l_{\alpha,max}$	0.122 m	0.122 m
Mean particle velocity in the spray zone $\bar{v}_\alpha$	0.781 m s^{-1}	0.778 m s^{-1}
Max. particle velocity in the spray zone $v_{\alpha,max}$	6.86 m s^{-1}	4.65 m s^{-1}
Mean particle velocity in the fluidised bed $v_{1-\alpha}$	0.426 m s^{-1}	0.639 m s^{-1}
Weibull-parameters a, b	$a = 0.09; b = 2.05$	$a = 0.077; b = 2.09$

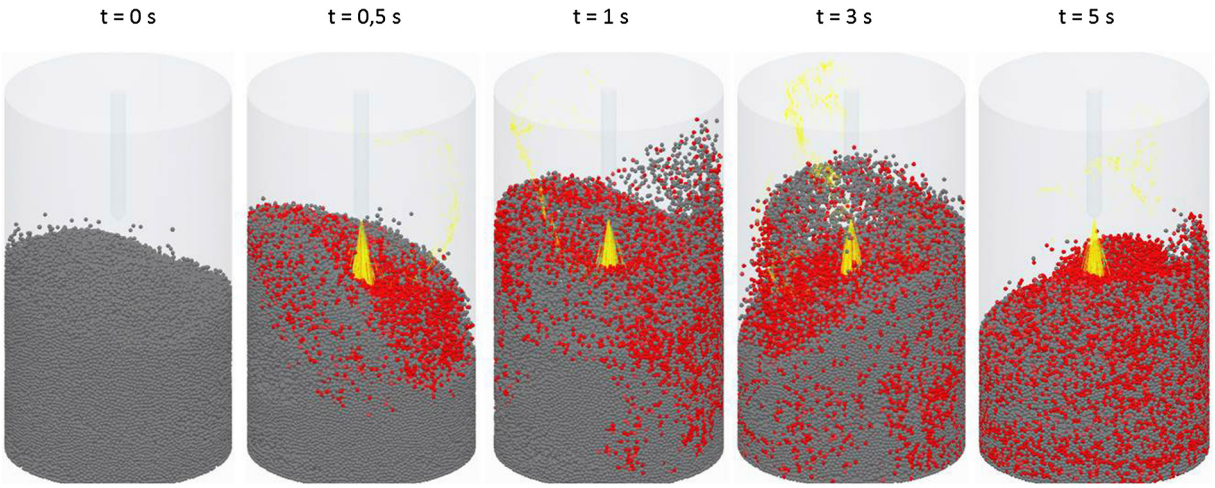

Fig. 11. Evolution of wet particle distribution in the fluidised bed. Gray particles are dry, red particles are wetted, collided with droplets and yellow particles are sprayed, discrete droplets illustrated as streamlines to make them visually observable. (For interpretation of the references to color in this figure legend, the reader is referred to the web version of this article.)

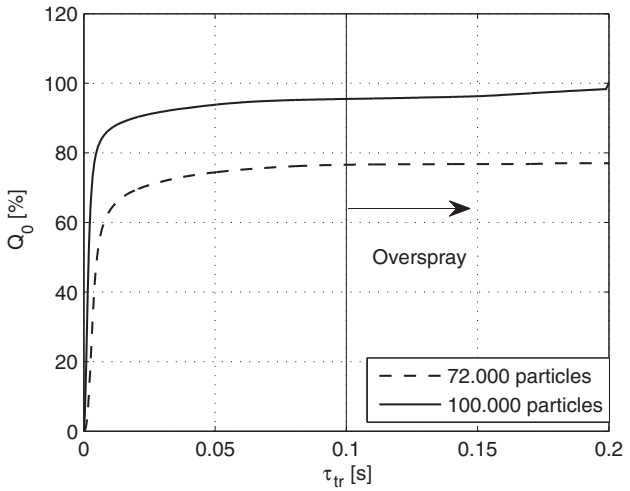

Fig. 12. Cumulative number distribution Q_0 of droplet existing time to derive the ratio of overspray for superficial gas velocity $u = 2 \cdot u_{mf}$ at two different particle numbers. With the lower number of particles a high gap between particles and spray nozzle is considered.

flow down into the fluidised particle bed. In the particle bed the droplets either collide with particles, leading to a successful wetting event at any time, or are discharged as overspray by a turning and deflected nozzle gas flow. Since all particle wetting events are recorded by counter variables, the wetting distribution in the fluidised bed can be visualised. Fig. 11 shows the wetted fluidised bed at different time steps. When a droplet collides with a particle, the particle changes its colour from grey to red. Starting with a completely grey particle bed the wetted, red particles in the top domains quickly move to the bottom of the fluidised bed and mix with the other dry particles. The mixing process is dominated by raising gas bubbles that induce the particle motion. The discrete droplets in Fig. 11 are illustrated as yellow streamlines. On the one hand yellow streamlines penetrate from the nozzle into the fluidised particle bed. On the other hand non-collided, oversprayed droplets can be observed in the freeboard domain. The ratio of overspray is changing over time and depends on gas bubble eruption in the freeboard which is in direct interference with the nozzle gas flow.

Not every droplet can deposit on the particle surface. Particularly for the top-spray configuration, where the nozzle gas flow is in counter-current to the fluidisation gas flow, droplets can be carried along with the fluidisation gas flow and had been discharged before a collision event could take place. The ratio of overspray determines the effectiveness of granulation. The loss of droplets reduces the particle growth with influence on the growth kinetics. From the discrete droplet simulation the ratio of overspray from the droplet existence time can be obtained. Those analyses were impossible in the previous experimental investigation.

Fig. 12 shows the cumulative distribution of the droplet existing time. After 0.1 s it can be concluded from the horizontal segment of distribution function that a droplet is discharged with very low probability of any further collision event. Droplets with 0.1 s existing time and more have already turned around their flow direction and move upwards through the upper freeboard domain. The time stamp has been identified as characteristic measure for the determination of the droplet existing time to compare overspray ratios. The ratio of overspray has been obtained with 4.49%, i.e. 95.51% of the droplets successfully collide with particles. The mean droplet existence time is 0.0026 s. In order to emphasise the impact of overspray in dependence on the process conditions a second simulation case has been set up. Besides the 100.000 particles a reduced number of 72.000 particles has been simulated, increasing the gap between the spray nozzle and the particle bed. As a consequence, more droplets are redirected and the ratio of overspray increases up to 23.4% at a mean droplet existence time of 0.0051 s.

Having a closer look at the spray zone domain, where the droplet-particle collisions take place, the wetting procedure can be described in differentiated manner. Fig. 13 shows a vertical cut through the spray zone sub-geometry at different time steps. The particle colour is here according to the number of successful particle-droplet collisions and therewith a measure of the moisture content. From the observation of particle-droplet collisions in the spray zone as well as from the previously discussed particle crossing length distribution three different types of particle wetting procedures can be derived:

- **Single particle wetting:** Widely distributed particles with high translational and rotational velocities are in intensive contact with sprayed droplets. A very high wetting degree, up to the wetting of the entire surface is achieved. These particles typi-

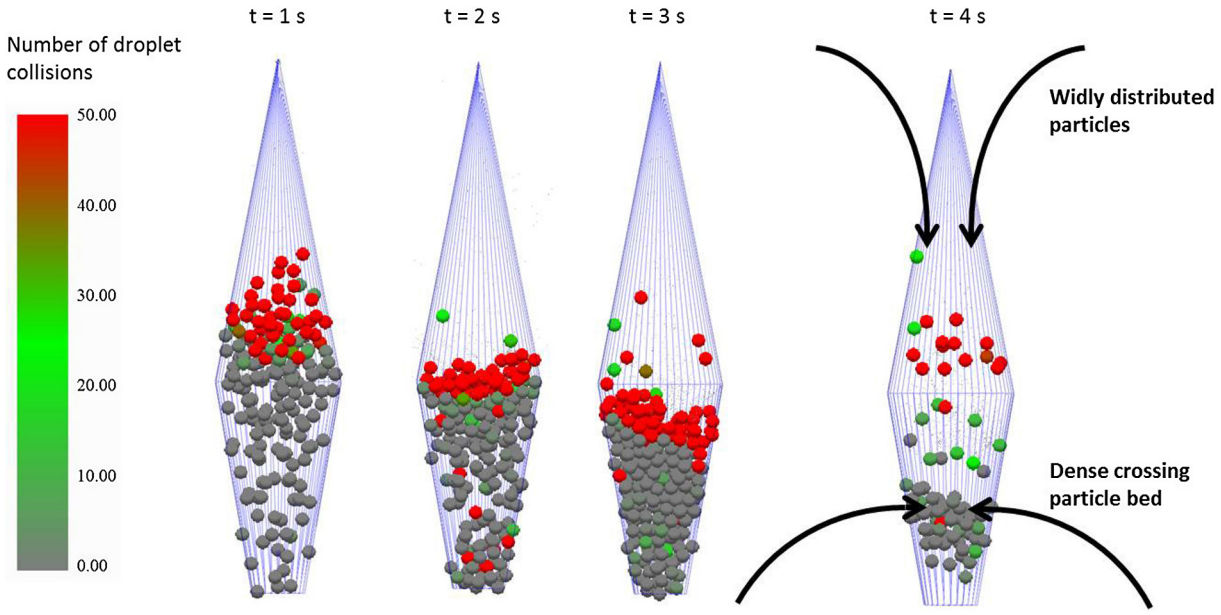

Fig. 13. Particle wetting in the extracted spray zone compartment for different particle distributions at different simulation times. The spray nozzle is located in top of the spray zone.

Table 5
Evaluation of simulation accuracy of mean particle residence time and mean solid volume fraction in the spray zone in comparison with the experimental results obtained in Börner et al. (2014).

Fl. velocity	Param.	Sim.	Exp.	Diff.
$u = 2 \cdot u_{mf}$	τ_α	0.0524 s	0.0412 s	21.4%
	α	$8.9 \cdot 10^{-4}$	$1.02 \cdot 10^{-3}$	14.6%
$u = 3 \cdot u_{mf}$	τ_α	0.0404 s	0.0323 s	20.1%
	α	$8 \cdot 10^{-4}$	$9.69 \cdot 10^{-4}$	22.1%

cally enter the spray zone from the top and cross until the bottom end. High nozzle mass flow rates, fluidisation velocities and bed masses increase the ratio of single particle wetting.

- **Bed surface wetting:** On average this area appears in the centre of the spray zone. Particles have low rotations speeds at high solid volume fractions. A unilateral and one-sided wetting of particles occurs. The upper layers of the dense crossing particle bed will be wetted in this way.
- **Sporadic and selective particle wetting:** Single particle-droplet collision occurs with partial wetting. Those are usually particles in the bottom area of spray zone. Only a few droplets can reach these domains during bubble eruption or low solid volume fraction in the spray zone.

On the right side of Fig. 13 the different particle entries into the spray zone are outlined. Particles entering at the top will experience single particle wetting. Sideways entering particles will either result in bed surface wetting or selective wetting. The wetted particles returned in the drying zone will exhibit a different agglomeration tendency according to the obtained moisture content in the spray zone. The likelihood of successful bridging and agglomerate formation with other particles increases with the amount of wetted surface area. Particle with high wetting degree have the ability to coalescence to several particles, whereas particles with low wetting degree have a reduced agglomeration tendency. The amount of particle wetting will thus have an influence on particle growth kinetics.

In order to compare the obtained results of the simulations, Table 5 shows the mean particle residence time and solid volume fraction in the spray zone of the simulations compared to the previous experimental outcomes (Börner et al., 2014). It can be seen that the mean particle residence times and the mean solid volume fraction deviate from 15% to 22%. This is in an acceptable range for the applied simulation approaches based on similarity models and confirms the applicability of scaling approach. Such deviations are in tolerance compared to the extreme time savings achieved by the scaling. Furthermore, particle residence times in the spray zone have been obtained by other authors as well. For instance Fries et al. (2011) obtained mean particle residence times (in a smaller apparatus and for higher fluidisation velocities) in an assumed spray zone geometry of $\tau_\alpha = 0.0245$ s, being in a similar range like values obtained from the current DEM-CFD studies and previously reported experimental results.

4. Conclusions

Particle and droplet motions in a top-spray fluidised bed have been investigated by DEM-CFD simulations having applied a similarity model. The similarity model resulted in a reduction of particle number and necessary simulation time while successfully maintaining the characteristics of fluid flow and particle-fluid interaction. The validity of the similarity model has been proven for a flat fluidised bed. The particle number in a cylindrical lab-scale fluidised bed has been reduced. Reasonable computation times have been achieved to simulate this large-scale multiphase system. A two-compartment approach has been applied, dividing the fluidised bed into a spray and drying zone. Particle residence time distributions and particle crossing length distribu-

tions in the spray zone as well as droplet existing times have been obtained for the three-phase flow. Within the spray zone not all particles behave in the same way. Distributed residence times and particle crossing length cause different particle wetting procedures that may influence the agglomeration tendency of particles and thus the particle growth behaviour. In the determination of particle growth in the spray zone, the distributive behaviour needs to be accounted for a more precise description. Today, only mean residence times have been accounted in compartment models not considering the distribution influence on the particle growth kinetics. Overspray ratios have been determined by closer examination of discrete droplets. The process conditions influence the ratio of overspray and are decisive for the efficiency of the overall process.

Acknowledgement

The authors gratefully acknowledge the funding of this work by the German Federal Ministry of Science and Education (BMBF) as a part of the InnoProfile project NaWiTec (03IP701X).

References

Antonyuk, S., Heinrich, S., Tomas, J., Deen, N., van Buijtenen, M., Kuipers, J., 2010. Energy absorption during compression and impact of dry elastic-plastic spherical granules. Granul. Matter 12, 15–47.

Börner, M., Peglow, M., Tsotsas, E., 2011. Particle residence times in fluidized bed granulation equipments. Chem. Eng. Technol. 34, 1116–1122.

Börner, M., Hagemeier, T., Ganzer, G., Peglow, M., Tsotsas, E., 2014. Experimental spray zone characterization in top-spray fluidized bed granulation. Chem. Eng. Sci. 116, 317–330.

Chaudhury, A., Armenante, M., Ramachandran, R., 2015. Compartment based population balance modeling of a high shear wet granulation process using data analytics. Chem. Eng. Res. Des. 95, 211–228.

Cundall, P., Strack, O., 1979. A discrete numerical model for granular assemblies. Géotechnique 29, 47–65.

Deen, N., van Sint Annaland, M., van der Hoef, M., Kuipers, J., 2007. Review of discrete particle modeling of fluidized beds: fluidized bed applications. Chem. Eng. Sci. 62, 28–44.

Di Felice, R., 1994. The voidage function for fluid-particle interaction systems. Int. J. Multiph. Flow 20, 153–159.

Fries, L., Antonyuk, S., Heinrich, S., Palzer, S., 2011. DEM-CFD modeling of a fluidized bed spray granulator. Chem. Eng. Sci. 66, 2340–2355.

Fries, L., Dosta, M., Antonyuk, S., Heinrich, S., Palzer, S., 2011. Moisture distribution in fluidized beds with liquid injection. Chem. Eng. Technol. 34, 1076–1084.

Fries, L., Antonyuk, S., Heinrich, S., Dopfer, D., Palzer, S., 2013. Collision dynamics in fluidised bed granulators: a DEM-CFD study. Chem. Eng. Sci. 86, 108–123.

Hoffmann, T., Peglow, M., Tsotsas, E., 2011. Prozessdynamik der wirbelschichtgranulierung. Chem. Ing. Tech. 83, 658–664.

Hussain, M., Kumar, J., Peglow, M., Tsotsas, E., 2014. On two-compartment population balance modeling of spray fluidized bed agglomeration. Comput. Chem. Eng. 61, 185–202.

Kunii, D., Levenspiel, O., 1991. Fluidization Engineering, Butterworth-Heinemann Series in Chemical Engineering. Butterworth-Heinemann, Boston.

Li, J., Freireich, B., Wassgren, C., Litster, J., 2012. A general compartment-based population balance model for particle coating and layered granulation. AIChE J. 58, 1397–1408.

Li, L., Remmelgas, J., van Wachem, B.G., von Corswant, C., Johansson, M., Folestad, S., Rasmuson, A., 2015. Residence time distributions of different size particles in the spray zone of a Wurster fluid bed studied using DEM-CFD. Powder Technol. 280, 124–134.

Link, J., Godlieb, W., Tripp, P., Deen, N., Heinrich, S., Kuipers, J., Schönherr, M., Peglow, M., 2009. Comparison of fibre optical measurements and discrete element simulations for the study of granulation in a spout fluidized bed. Powder Technol. 189, 202–217.

Mindlin, R.D., Deresiewicz, H., 1953. Elastic spheres in contact under varying oblique forces. Trans. ASME Ser. E J. Appl. Mech. 20, 327–344.

Mio, H., Akashi, M., Shimosaka, A., Shirakawa, Y., Hidaka, J., Matsuzaki, S., 2009. Speed-up of computing time for numerical analysis of particle charging process by using discrete element method. Chem. Eng. Sci. 64, 1019–1026.

Radeke, C., Glasser, B., Khinast, J., 2010. Large-scale powder mixer simulations using massively parallel GPUarchitectures. Chem. Eng. Sci. 65, 6435–6442.

Sakai, M., Koshizuka, S., 2009. Large-scale discrete element modeling in pneumatic conveying. Chem. Eng. Sci. 64, 533–539.

Sakai, M., Abe, M., Shigeto, Y., Mizutani, S., Takahashi, H., Vire, A., Percival, J., Xiang, J., Pain, C., 2014. Verification and validation of a coarse grain model of the DEM in a bubbling fluidized bed. Chem. Eng. J. 244, 33–43.

Sherony, D.F., 1981. A model of surface renewal with application to fluid bed coating of particles. Chem. Eng. Sci., 845–848

Sutkar, V.S., Deen, N.G., Patil, A.V., Salikov, V., Antonyuk, S., Heinrich, S., Kuipers, J., 2016. CFD–DEM model for coupled heat and mass transfer in a spout fluidized bed with liquid injection. Chem. Eng. J. 288, 185–197.

Suzzi, D., Toschkoff, G., Radl, S., Machold, D., Fraser, S.D., Glasser, B.J., Khinast, J.G., 2012. Dem simulation of continuous tablet coating: effects of tablet shape and fill level on inter-tablet coating variability. Chem. Eng. Sci., 107–121

Thakur, S.C., Ooi, J.Y., Ahmadian, H., 2016. Scaling of discrete element model parameters for cohesionless and cohesive solid. Powder Technol., 0032-5910 293, 130–137. http://dx.doi.org/10.1016/j.powtec.2015.05.051.

Turchiuli, C., Jimenèz, T., Dumoulin, E., 2011. Identification of thermal zones and population balance modelling of fluidized bed spray granulation. Powder Technol. 208, 542–552.

Washino, K., Hsu, C., Kawaguchi, T., Tsuji, Y., 2007. Similarity model for DEM simulation of fluidized bed. J. Soc. Powder Technol. Jpn. 44, 198–205.

Wnukowski, P., 1989. The coating of particles in a fluidized bed (residence time distribution in a system of two coupled perfect mixers). Chem. Eng. Sci., 493–505